

# *Physical Simulation as a Tool to Evaluate the complex Microstructure of Microalloyed Railroad Wheels*

Solange Tamara da Fonseca<sup>1a\*</sup>, Andrei Bavaresco Rezende<sup>1b</sup>, Clelia Ribeiro de Oliveira<sup>1c</sup>,  
Domingos Jose Minucucci<sup>2d</sup>, Paulo Roberto Mei<sup>1e</sup>

a. [tamara@fem.unicamp.br](mailto:tamara@fem.unicamp.br), b. [abavaresco@fem.unicamp.br](mailto:abavaresco@fem.unicamp.br), c. [clelia.rib@hotmail.com](mailto:clelia.rib@hotmail.com)  
d. [domingosminucucci@terra.com.br](mailto:domingosminucucci@terra.com.br), e. [pmei@fem.unicamp.br](mailto:pmei@fem.unicamp.br)

\* corresponding author

<sup>1</sup> University of Campinas, Faculty of Mechanical Engineering, Campinas, 13083-860, Brazil

<sup>2</sup> DJ Consulting, Botucatu, SP, Brasil

Keyword: Microalloyed railway wheel, niobium, heavy haul.

## **Abstract**

Pearlitic microstructures are commonly used in the manufacture of wheels, due to high wear resistance, combined with good ductility and fracture toughness. However, recent studies with bainitic microstructures reveal better performance in wear and rolling contact fatigue. In 2013, AAR (Association of American Railroads) introduced a new class of microalloyed steel called Class D as acceptable for heavy haul load transport. The new Class D steel must have the same chemical composition as Class C steel with the small addition of alloying elements to provide the required hardness and mechanical properties. The addition of microalloying elements to the manufacturing process can provide different microstructures in the railroad wheels. To identify the microstructures existing in microalloyed steel and compare them with wheel microstructures, physical simulations were conducted using Gleeble equipment. Microstructural characterizations, x-ray diffraction (XRD) and hardness were evaluated in order to isolate the present phases. The hardness map shows the range hardness of each microstructure and it is possible to correlate these with wheel hardness. The pearlitic, ferritic and martensitic microstructures were easily identified by microscopy. The bainitic microstructure was identified by hardness values and microscopy. The austenitic microstructure was identified by XRD. Physical simulation is effective to produce microstructures at different rates and temperatures in a controlled form which is possible to be investigated.

## **1. Introduction**

A railway wheel and axles are crucial parts in the safe operation of rail transport, as they support the entire weight of the cars. High reliability is required in terms of resistance; therefore, this is one of the most important and fundamental characteristics in the development of new materials [1-3].

Pearlitic microstructures are commonly used in the manufacture of wheels, due to high wear resistance, combined with good ductility and fracture toughness. The thickness of the lamellas in the pearlitic microstructure can be controlled by both alloying elements and by the cooling rate [4-7]. So far, research has focused mainly on the pearlitic microstructure and its effect on the wear properties of the wheel [8, 9]. However, recent studies with the bainitic microstructure reveal better wear performance and rolling contact fatigue. [4, 10-13].

For load transportation, medium carbon steel (eutectoid steel) called Class C (AAR) are generally used in the manufacture of railway wheels. In 2013, AAR introduced a new class of microalloyed steels called Class D as acceptable for heavy haul load transport. The hardness of the rim must show a values range of 341-388 BHN for Class D, greater than the hardness range in Class C; which is 321-363 BHN. In addition, the new Class D steel must have the same chemical composition as Class C; with only small additions of alloying elements to provide the required hardness [6, 15-18].

The manufacturing process for railway wheels is complex and well described in the literature [2, 5, 18]. After metal formation, the wheel is heated to approximately 900 °C (austenitization temperature) and the wheel tread (exclusively) is quickly quenched with water (Figure 1). Surface quenching reduces the pearlite interlamellar spacing in regions close to the surface, increasing its hardness and resistance to wear. The wheel is then left to thermalization in the air before a tempering treatment. Contraction and expansion of the wheel during quenching cause residual stresses in it. After cooling, the wheel is tempered to approximately 500 °C. This process reduces the levels of residual stress imposed by previous treatment and guarantees the presence of compressive stresses in the wheel circumference that are known to help prevent the formation of crack fatigue during service [2, 19]. At the end of this process, the wheel's tread is machined to remove the fragile tempered martensite layer and ensure a uniform microstructure of ferrite and pearlite in the section of the wheel rim. However, if cooling conditions are not controlled perfectly, a microstructure different from pearlite may coexist. Commonly a mixture of perlite and bainite will be present in regions close to the tread and flange of the wheels even after the final machining [18]. The alloy design is important because it will control the thickness of the martensite layer and thus guarantee a ductile and toughness microstructure in the rim region [9].

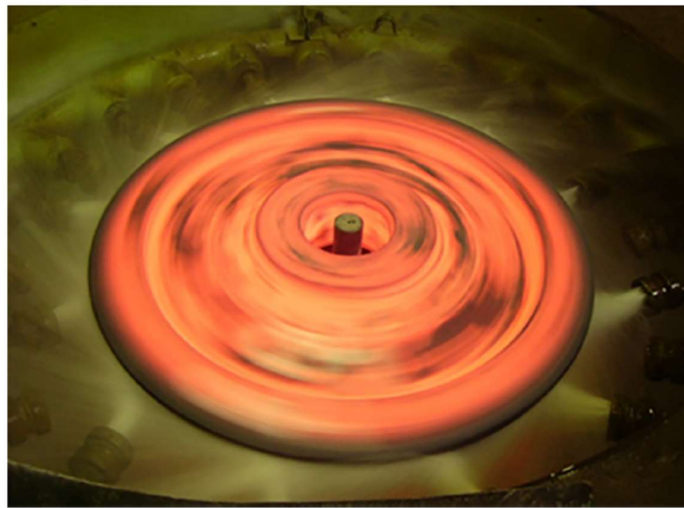


Figure 1: Wheel rim subjected to water quenching treatment [5].

During the tempering and quenching process, the wheel's tread may experience different temperature peaks and cooling rates, resulting in a complex mixture of phases over the wheel's profile (Figure 2) from tread to rim. For this reason, it is important to understand mixed and complex microstructures through continuous cooling (CCT) and isothermal treatment [4, 18].

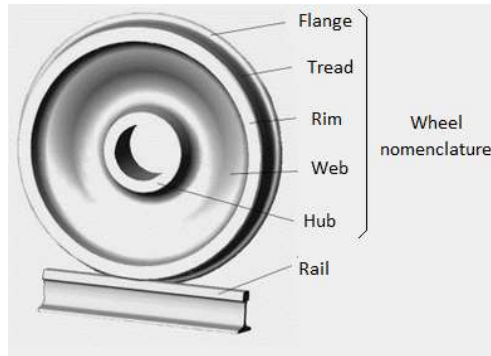


Figure 2: Nomenclature of railroad wheels indicating analysis regions: rim and tread.

During heating or cooling, different microstructures can appear in medium carbon steel, such as ferrite (F), retained austenite (A), cementite ( $Fe_3C$ ), pearlite (ferrite and cementite), bainite (ferrite and cementite) and martensite. Retained austenite can be confirmed by X-ray diffraction; pearlite, ferrite and martensite are well known for continuous cooling and are easy to identify by microscopy and hardness. On the other hand, the bainite and MA (Martensite/Austenite) are much more difficult, requiring the application of other techniques, such as Transmission Electron Microscopy [20-21]. Dilatometry associated with metallographic analysis and hardness tests allows a better understanding of the structure of these materials. Table I indicates the hardness range of different microstructures for medium carbon steels and will be used to compare the results obtained in this work.

Table 1: Chemical composition of experimental alloys in wt. % and Vickers hardness

Reference	Elements (wt. %)					Hardness (HV)		
	C	Si	Mn	Nb	Others	Pearlite	Bainite	Martensite
[20]	0.69	-	-	-	-	210-355	250-650	-
[21]	0.80	0.25	0.48	-	Cr=0.20	415-430	-	-
[22]	0.75	0.63	0.91	-	-	300-359	-	705-787
[23]	0.45	2.08	2.69	-	-	-	420-600	750-770
[24]	0.76	0.23	0.72	-	-	260-340	-	-
[25]	0.74	0.30	0.83	0.05	Cr=0.22	338-358	-	-
[26]	0.83	1.9	2.3	0.02	Cr=1.44	370-390	610-635	730-750

This work shows an experimental effort to obtain, under controlled conditions, different microstructures using experiments of continuous cooling and isothermal treatment with the thermal-mechanical physical Simulation System. The results were compared with the microstructure of a Class C railway wheel.

## 2. Materials and Methods

In this study a 7Nb microalloyed eutectoid steel (AAR Class D) was obtained from a forged railway wheel. The chemical composition is shown in Table II. Some results of 7C eutectoid steel (AAR Class C) were used for comparison [27]. Chemical analysis was performed using an electric arc optical emission spectrometer.

Table 2: Chemical composition of steels (wt. %)

Steel	C	Si	Mn	Ni	Mo	Cr	Nb
7C [27]	0.68	0.34	0.83	0.054	0.015	0.21	0.008
7Nb	0.63	0.31	0.83	0.12	0.11	0.36	0.014

Cylindrical samples with a reduced section diameter of 5 mm and a free space of 5 mm were used in the physical simulations in a Gleeble 3800 thermomechanical simulator. The thermal cycle was controlled by resistive heating, using a type K thermocouple and the volumetric phase transformations were measured with a contact dilatometer. The tests with continuous cooling used cooling rates from 0.5 to 100 °C/s. Isothermal transformation experiments (TTT) were carried out to produce specific microstructures such as pearlite and bainite. These samples were previously austenitized at 880 °C for 300 s using a heating rate of 0.16 °C/s, then they were cooled at a rate of 20 °C/s until reaching the temperature of the isothermal treatment at 300, 400, 500 and 600 °C. All samples were sectioned in the center of the section and prepared metallographically by polishing with a diamond suspension up to 1 μm. The microstructure was revealed by chemical attack with Nital (2% aqueous solution of nitric acid in ethanol).

Vickers microhardness mapping was performed with a LM100AT (LECO) equipment. A load of 200 kgf was applied for 15 s with a spacing of 500 μm between the indentations. Nanoindentation tests were performed on samples treated by continuous cooling at rates at the 1, 3, 5, 10 and 100 °C/s and samples treated isothermally at 300 and 400 °C. The parameters used were a peak load of 1000 μN loading rate of 200 μN / s using a self-similar pyramidal Berkovich indenter. The presence of retained austenite was confirmed by XRD with Panalitical X'pert Pro equipment, operating at 40 kV with CoK $\alpha$  radiation. For the characterization of the morphology and identification of precipitates, the transmission electron microscope (MET) FEI Company, model Tecnai G2F20, from the Structural Characterization Laboratory of UFSCar was used. The samples were prepared by electrolytic polishing with a 25% perchloric acid solution in ethanol with the application of a voltage of 12 V and a current of 2.2 A.

### 3. Results

#### 3.1 Microalloyed Railroad Wheel Microstructures

The microstructures of the cross section of the 7Nb railroad wheel are shown in Fig.3a-h. In addition, Fig. 4 shows the hardness map and ferrite fractioning in the cross section of the rim of the 7C and 7Nb wheels.

The standards applicable to wheels used in heavy transport operations in Brazil are based on the M-107 / M-208 standard of AAR, which does not specify acceptable microstructures, except that the wheel must be free of martensite [28].

The initial microstructure near the tread (0 to 3 mm) is composed of a mixture of phases, including: grain boundary ferrite (GBF) and polygonal ferrite (PF), upper bainite (UB) and lower bainite (LB) (Fig 3a-b). As it is a complex heat treatment, the morphology of bainite is not easily distinguishable; however, Li et. al, presents an upper bainite microstructure quite similar to that presented in this work.

Between 6 and 9 mm (Fig. 1c-d) of the tread, the microstructural characteristics are similar but some start the formation of the pearlite and the GBF increases with depth. At 12 mm (Fig. 3e), we have a microstructure with regions of ferrite and cementite of nearly the same orientation which are

typical of degenerate pearlite (DP) in addition to grains of PF and UB [30]. At 15 mm (Fig. 3f-h) we can observe only ferrite and pearlite (P) grains, which are expected microstructures for the chemical composition of this steel.

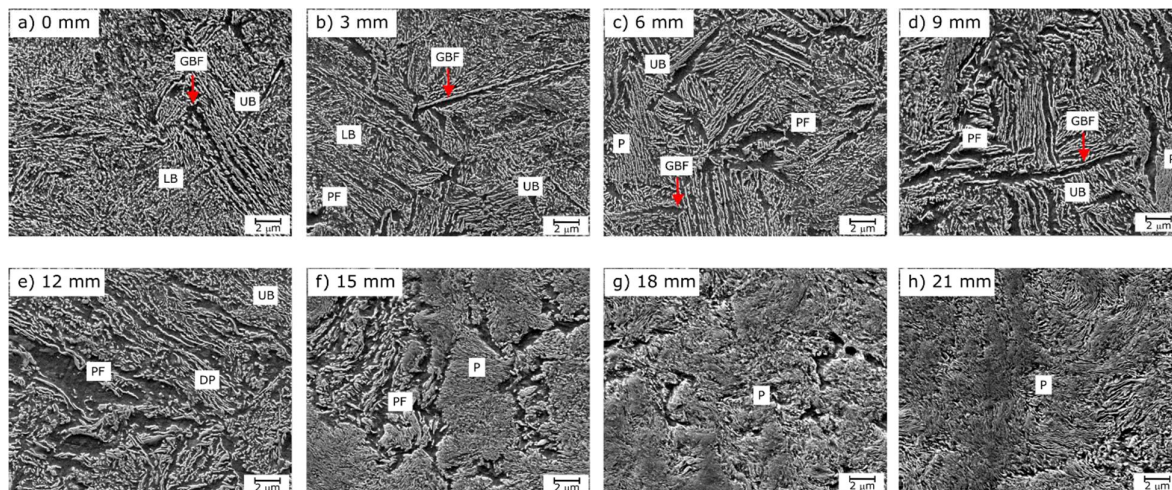


Figure 3: Wheel 7Nb microstructure cross section as seen from the rim. Observed microstructures: grain boundary ferrite (GBF), polygonal ferrite (PF), lower bainite (LB), upper bainite (UB), degenerated pearlite (DP) and pearlite (P).

The presence of ferrite was also observed in the hardness map, where we noticed a drop in hardness and an increase in the ferrite fractioning (Fig. 4). However, the increase of ferrite fractioning in the steel occurred due to the addition of Mo, which helped to stabilize the ferrite phase.

The quenching of the wheel rim promoted a mixture of phases in 7Nb steel, which reflected an increase in the initial hardness when compared to 7C steel.

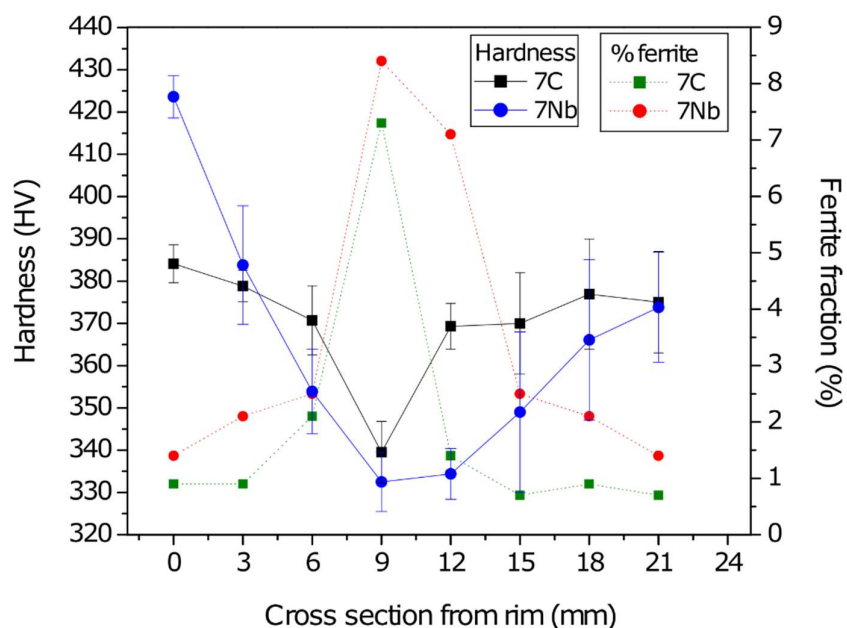


Figure 4: Hardness map vs ferrite fractioning as observed from the wheel rim of 7C and 7Nb steels.

Niobium is used as alloying element for precipitation hardening and grain refining in steels [31]. In this work, niobium contributed to the grain refining of austenite. TEM analysis (Figure 5) shows the presence of fine niobium carbides (50 nm) in the wheel's microstructure. Due to the precipitate size it was not possible to find the selection area diffraction on the axis zone of these precipitates. Thus, the EDS technique confirmed presence of niobium.

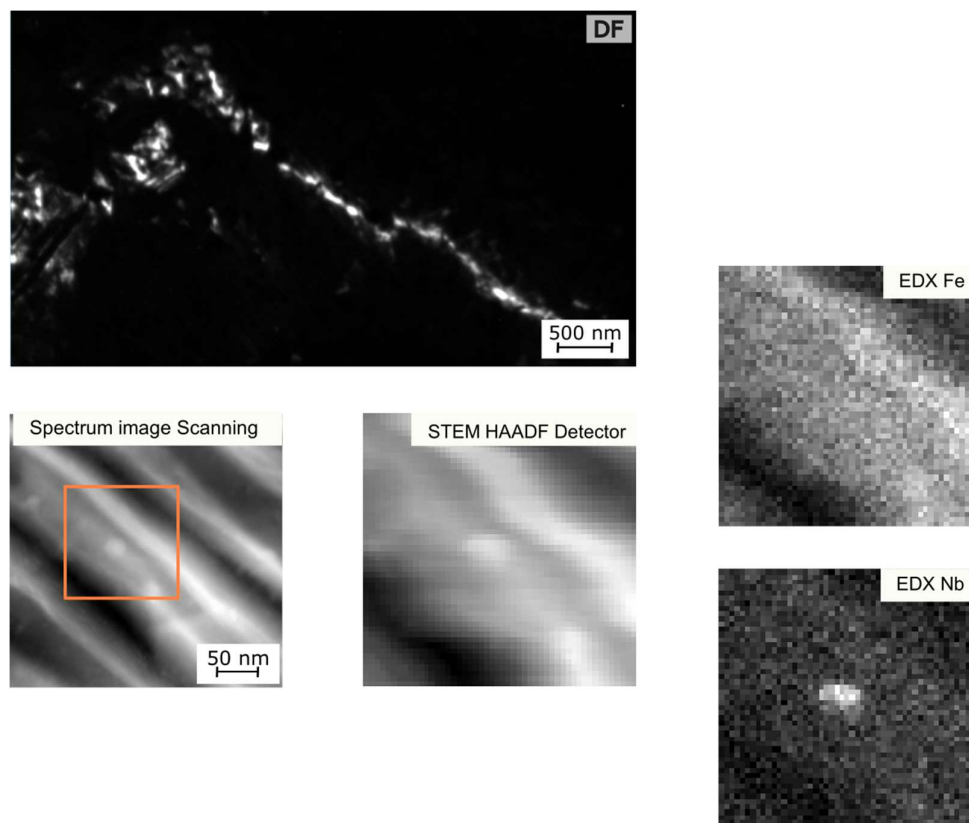


Figure 5: Micrographs of 7Nb steel showing niobium carbide precipitates along the grain boundaries in the Dark Field, HAADF and EDX.

## 3.2 Physical Simulation

### 3.2.1 Continuous Cooling Transformation Tests

The diagram of the continuous cooling transformation (CCT), together with the hardness and resulting microstructures are shown in Fig. 6. The variation in the start (Ar3 - blue squares) and end (Ar1 - blue circles) temperatures of the austenite decomposition was plotted according to their respective cooling rates. The CCT diagram, shows a decreasing trend in Ar3 and Ar1 temperatures was observed as cooling rates increased. Fig. 7 shows some microstructures obtained for the most relevant cooling rates in the CCT diagram. The cooling rates of 0.5 and 1 °C/s (Fig. 6a-b) resulted in microstructures composed mainly of pearlite (P) and some GBF. At the rate of 1 °C/s there is greater refinement of the pearlite compared to the rate of 0.5 °C/s, which resulted in a higher hardness value ( $307 \pm 17$  HV and  $336 \pm 16$  HV for 0.5 and 1 °C/s, respectively). Between 3 and 5 °C/s (Fig. 6c-f), there is a mixture of phases composed of P, ferrite matrix with Fe<sub>3</sub>C needles (B) and martensite plates, which caused an increase in hardness to values of 410 and  $592 \pm 55$  HV, respectively. The

high dispersion presented in the hardness deviation ( $\pm 55$  HV) reveals signs of the presence of multiphase microstructures [29, 32]. For a cooling rate of  $10\text{ }^{\circ}\text{C/s}$  (Fig. 6g-h) we have a microstructure composed of martensite-austenite (MA) with some grains of bainite, and the hardness of  $733 \pm 59$  HV was higher than the other rates. The samples cooled above  $20\text{ }^{\circ}\text{C/s}$  (Fig. 6i) are mainly composed of MA with hardness above  $809 \pm 10$  HV.

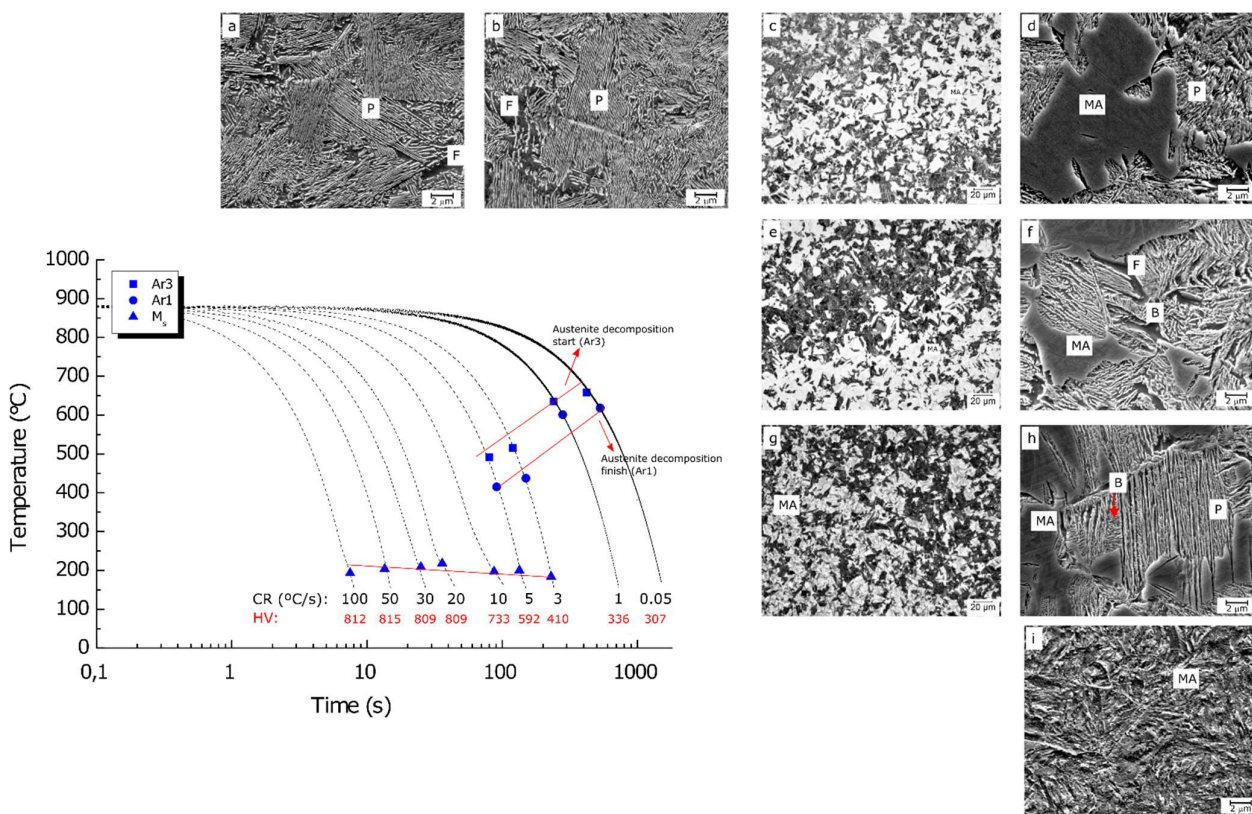


Figure 6: Continuous cooling transformation (CCT) diagram showing the variation of the Ar3 and Ar1 transformation temperatures as a function of the cooling rate (CR). The resultant Vickers hardness is reported after each cooling cycle. The corresponding microstructural characterizations are presented for:  $0.5\text{ }^{\circ}\text{C/s}$  (a);  $1\text{ }^{\circ}\text{C/s}$  (b);  $3\text{ }^{\circ}\text{C/s}$  (c-d);  $5\text{ }^{\circ}\text{C/s}$  (e-f);  $10\text{ }^{\circ}\text{C/s}$  (g-h) and  $100\text{ }^{\circ}\text{C/s}$  (i). Etched with Nital 2 %. (a, b, d, f, h, i) SEM images and (c, e, g) optical images. Observed microstructure: martensite-austenite (MA), bainite (B), Ferrite (F) and Pearlite (P).

Fig. 7 compares some dilatometry curves during heating and cooling of 7Nb and 7C steels to evaluate the effect of an alloy element addition on the variation of the start (Ac1) and end (Ac3) temperatures of ferrite to austenite transformations during heating, as well as the start (Ar3) and end (Ar1) temperatures of austenite decomposition during cooling (indicated by blue arrows). During heating, Ac1 and Ac3 were practically similar at all rates; that is, the alloying element did not cause a delay in the formation of austenite. On the other hand, during cooling, we have noticed significant differences, especially at the rate of  $3\text{ }^{\circ}\text{C/s}$ . During the dilatometry test performed at  $1\text{ }^{\circ}\text{C/s}$  (Fig. 7a), Ar3 was found at  $630\text{ }^{\circ}\text{C}$  and  $640\text{ }^{\circ}\text{C}$ , and Ar1 at  $608\text{ }^{\circ}\text{C}$  and  $660\text{ }^{\circ}\text{C}$  for 7Nb and 7C, respectively. Considering the microstructure received as the initial state of zero expansion, a residual contraction condition with a dimensional change of about  $1\text{ }\mu\text{m}$  was obtained after cooling to room temperature.

In addition, the Ar1 temperature was much lower in 7Nb steel (608 °C), which results in the formation of thinner cementite lamellae that show increased hardness [33].

In 7Nb steel for cooling rates of 3 and 5 °C/s, we have contraction values of 6 mm and the presence of two inflection points in the dilatometer curve which indicates the presence of multiphase microstructure. Analyzing the microscopic images, the presence of martensite plates, pearlite grains and regions composed of a ferrite matrix with carbide needles with a certain orientation (characteristic of a bainitic microstructure) are noted. On the other hand, in 7C steel, only ferrite and pearlite grains are present. The addition of Nb, Cr and Mo contributed to lowering of the Ar3 and Ar1 temperature (indicated by the blue arrows), which represents an increase in hardenability. The addition of Nb refined the austenitic grain size, which consequently caused an increase in nucleation sites, which accelerated the diffusion transformations and favored the reduction in the size of the bainite beams [31, 34].

In cooling rates above 10 °C/s we observe the expansion of the material to values of 8 mm, characteristic of the martensitic structure. In 7Nb steel, the microstructure has martensite plates and regions with needle-shaped carbides and the hardness values are high, which confirms the presence of these microconstituents (martensite and bainite). In the 7C steel, the hardness values are lower and there is an inflection of the curve at around 600 °C, indicating the presence of other constituents such as pearlite and ferrite, in addition to martensite and bainite.

Evaluating the microstructures for each cooling rate, it is not possible to correlate these with the microstructures observed in the wheel at the initial depths (0 to 12 mm) (Fig. 3). However, Rasouli, et al. investigated the effect of the cooling rate and strain temperature on microalloyed steels. It was observed that some rates produce a mixed microstructure of bainite and martensite [29], which corresponds to the microstructure found in the wheel between 0 and 3 mm from the tread. Minicucci et al. state that during the quenching process of the tread, at depths between 5 and 10 mm the cooling rate varies between 1.5 and 3 °C/s and for 15 mm the rate varies from 1.5 to 2.5 °C/s. Thus, using the CCT curve at a rate of 3 °C/s, the microstructure of 7Nb steel is composed of pearlite, bainite and martensite, and after a tempering process, this microstructure would be composed of pearlite, bainite and tempered martensite. Note that at 6 and 9 mm tread depth (Fig. 3c-d) the microstructures present (pearlite, ferrite and bainite) are similar to this. At greater depths, such as 12 and 15 mm, where the cooling rate was lower, it is noted that the microstructure is composed of a majority of pearlite and ferrite, in accordance with the microstructure shown in cooling rate of 1 °C/s of the CCT diagram [5].

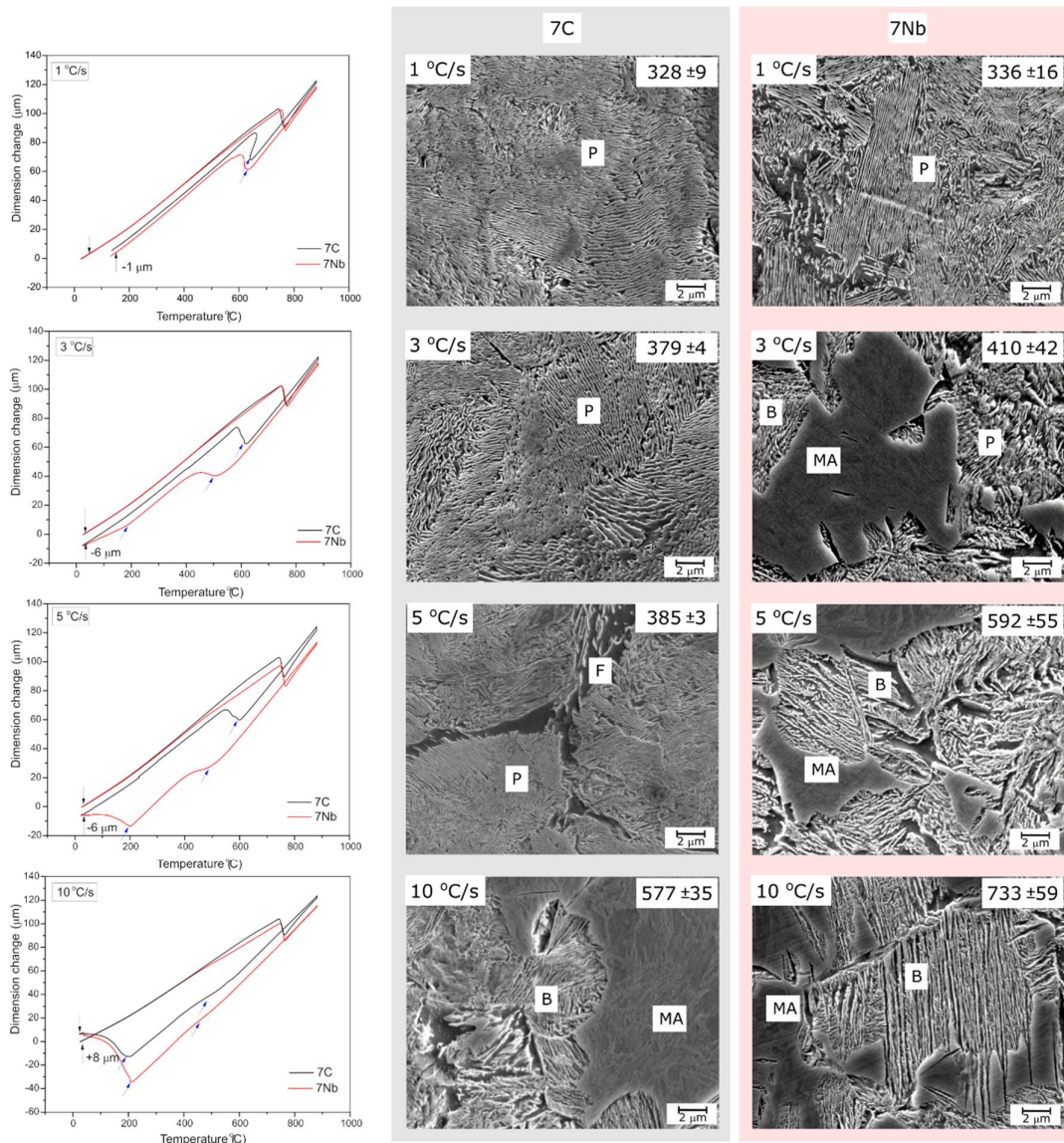


Figure 7: Dilatometric heating and cooling curves showing the variation of Ar3 and Ar1 transformation temperatures as a function of the 7C and 7Nb steel for some cooling rates and their micrographs. GBF – grain boundaries ferrite; B – bainite; MA – martensite and austenite.

X-ray diffraction was used to confirm the presence of austenite retained in samples of martensitic microstructure obtained in the dilatometry test (Figure 8). Note that after 5 °C/s the peak of austenite retained in the diffractogram is evident. For rates lower than 3 °C/s, the fraction of austenite is small; therefore, it was not detectable by this technique [35].

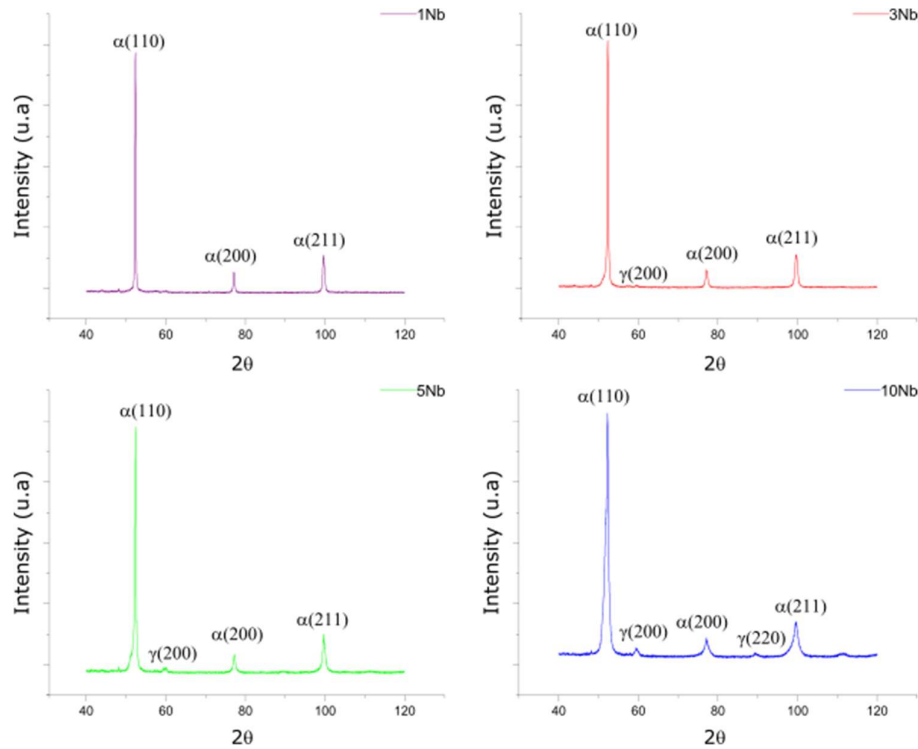


Figure 8: XRD pattern at different cooling rates 1; 3; 5; 10 °C/s:  $\alpha$  – ferrite (martensite) and  $\gamma$  – austenite.

### 3.2.2. Time Temperature Transformation Experiments

Figure 9 shows the results of the microstructure and phase transformation after rapid cooling and isothermal transformation at different temperatures. The expansion curves for the isothermal cycles as a temperature function are shown in Figure 9. The isothermal expansion and absence of additional expansion after cooling show the complete isothermal transformation for the studied thermal cycles of 300, 400, 500 and 600 °C. The micrographs shown in Figure 9 indicate the microconstituents present in the studied isotherms. At the isothermal temperature of 300 °C, the ferrite matrix with cementite carbides precipitated inside are typical of the lower bainite microstructure (LB) [36, 37]. At 400 °C there is a mixture of upper bainite (UB) and some grains of lower bainite (LB) [37-39]. The micrographs reveal a variation in the size of the ferrite and carbide needles, showing that the thickness of the bainitic ferrite and of carbide needles are proportionate to the transformation temperature, as size increases with temperature increase [40].

At 500 °C we have a transition microstructure composed of some grains of degenerate pearlite (DP), polygonal ferrite (PF), carbides aligned in the grain boundaries (this microstructure is similar upper bainite microstructure) [37, 41-43]. At 600 °C we have a microstructure mostly composed of pearlite (P) and some regions of degenerate pearlite.

As previously mentioned, the wheels undergo a tempering treatment at a temperature of 500 °C. It should be noted that the martensite / austenite constituent obtained closest to the tread due to the quenching process after being tempered at 500 °C would transform into tempered martensite and a mixture of pearlite, bainite and ferrite. This mixture can be correlated with the microstructure found

closest to the trend in Fig. 3a-d and is completely different than the microstructures shown in the isothermal treatment at 500 °C.

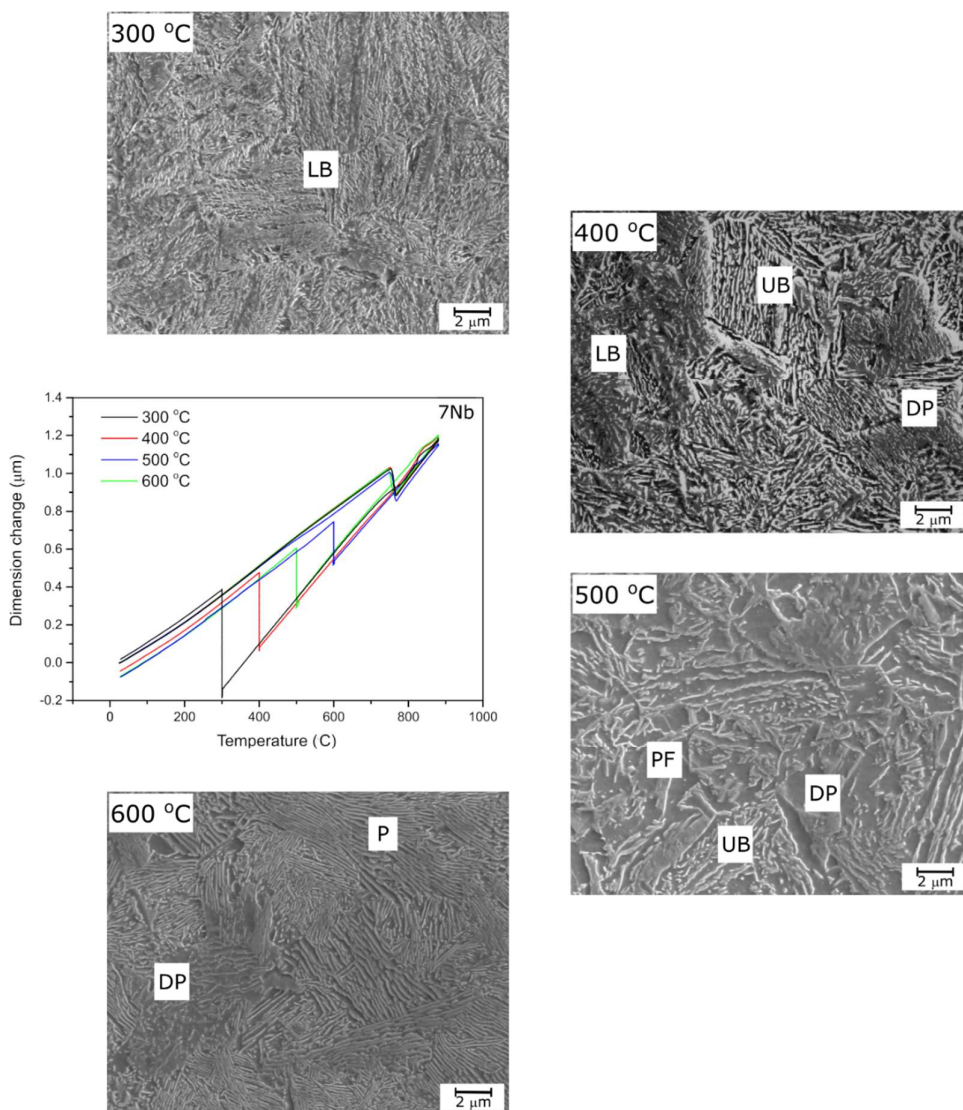


Figure 9: Dilatometry curves of isothermal treatments at different temperatures and micrographs of these (Nital attack 2%): P - pearlite; DP - degenerate pearlite; UB - upper bainite; LB - lower bainite and PF - polygonal ferrite.

Figure 10 shows a summary of the results in terms of hardness and microstructure as a function of thermal cycles. The hardness ranges were divided into 3 blocks to represent the microstructures: GBF + P (gray), UB + LB (green) and MA (pink). There is a correlation between the microstructures of CCT and ITT diagrams and hardness. For slow cooling rates up to 1 °C/s in continuous cooling and high isothermal treatments starting at 500 °C, we have a formation of F + P. The formation of B benefited from the increase in the cooling rate from 3 °C/s up to 10 °C/s or by isothermal transformations between 400 and 300 °C. The morphology of the bainite packets and their ferrite plates has become more straight and elongated for faster cooling rates from 5 °C/s. In addition, PF was observed only in the isothermal transformation at 500 °C. Although bainitic microstructures have

also been observed for isothermal cycles of rapid cooling below 500 °C, a difference in morphology and hardness can be observed, and we have concluded that at 400 °C there is presence of superior bainite and at 300 °C there is a microstructure composed mostly of lower bainite.

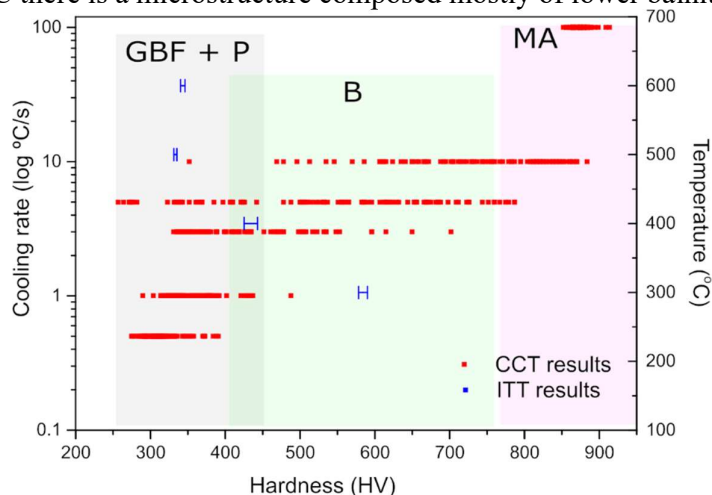


Figure 10: Microstructures and hardness as a function of the thermal cycle. GBF – grain boundaries ferrite, P – pearlite (lamellar and degenerate), B – bainite (upper and lower) and MA – martensite and austenite.

Figure 11 shows the nanohardness results for some cooling rates of the CCT cycle and isothermal treatment. The pearlitic microstructure showed a hardness value around 5.5 GPa, which is consistent with values found by Debehets et. al. When evaluating the nanohardness of a eutectoid steel with different thicknesses of pearlite interlamellar spacing, the result indicated a variation of 2 to 5 GPa in the samples treated with different temperatures within the pearlitic field [44]. Lan evaluated the effect of austempera on nanobainitic medium carbon steels (0.82% C) and found hardness values for bainite ranging from 7 to 10 GPa. In this work, the values found for the lower bainite was around 6.9 GPa, and the upper bainite around 5.7 GPa [45]. The martensite had a hardness of 11.4 GPa. There is great dispersion in the hardness values for the cooling rates of 3 to 10 °C/s, which confirms the existence of multiphases microstructure and that these can coexist in the product final of railway wheels.

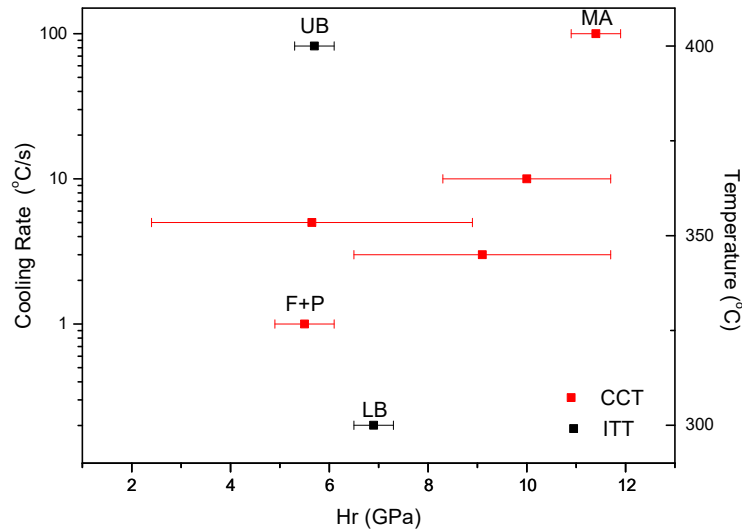


Figure 11: Nanohardness as a function thermal treatment. UB – upper bainite; LB – lower bainite, F – ferrite and P – pearlite.

Figure 12 shows a comparison in terms of microstructural characteristics and hardness between the profiles of a railway wheel based on the results obtained by physical simulation. Each profile of a railway wheel comprises a microstructure composed of pearlite and ferrite. However, the region close to the surface (orange arrow) exhibits superior hardness. As in this region the wheel has a cooling rate between 1 and 3 °C/s (data measured by Miniccuci, et al.), there is possibly a mixture of pearlite, bainite and martensite / austenite. After this microstructure is submitted to tempering process (at 500 °C), the martensite / austenite fraction is transformed into tempered martensite with the pearlite and bainite remaining. Thus, a mixture of microconstituents with different hardness is evident in this region.

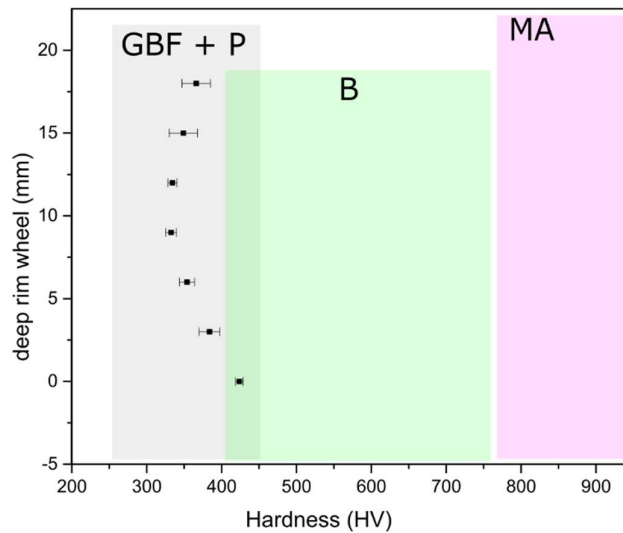


Figure 12: Railway wheel hardness profile (from the 0 mm tread) and correlation with the hardness regions of the microstructures obtained through continuous cooling and isothermal treatments.

Although this mix of microstructures is beneficial for increasing the hardness in Class D railway wheels, a loss in wear resistance and RCF can be found when they are in operation. Li, et. al. compared the performance of a wheel composed of pearlite, ferrite and upper bainite with a wheel composed only of pearlite and ferrite in disc-to-disc wear tests. The upper bainite aggravated the spalling defects in the wheel and this resulted in a greater loss of mass. They observed that with an increase one a number of cycles, the degree of fracture of the upper bainite is more severe than of the pearlite and this results in microcracks on the contact surface and these cracks join to form spalling, thus increasing the wear [4]. Liu et al. and Hu et al. also reported that the presence of different phases in the wheel (mainly ferrite) acts to provide a dissociation between phases of lesser and greater hardness. This dissociation promotes the appearance of microcracks in the deformed layer, which generates preferential regions of crack propagation and more wear [46-47]. Kalousek, et al. compared the wear of pearlitic, bainitic and tempered martensite steels with hardness ranging from 38 to 45 HRC and concluded that the wear rate depends strongly on the initial hardness for tempered martensite, moderately for bainite, and does not change significantly for pearlite. The lowest wear rate was obtained for all hardnesses of the pearlite, more than for tempered martensite or bainite with a hardness of 45 HRC. That is, the initial microstructure is important, as it will directly influence the wear rate on a first-life wheel [48].

#### **4. Conclusions**

A series of CCT and ITT experiments were carried out through physical simulation, in order to produce and isolate specific microstructures in a controlled manner. The results were useful to understand the mixed and complex microstructures produced by the heat treatments that the railway wheels are subjected to. The main conclusions are:

- The addition of alloy elements (such as Nb and Mo) favored the formation of bainite and martensite in shorter times, which occurred from the rate of 3 °C/s in contrast with steel without these, additions.
- Physical simulations performed for low cooling rates between 0.5 and 1 °C/s showed a soft matrix composed of ferrite and pearlite. These microstructures are present in the railway wheel at a depth of 15 mm.
- Cooling rates of 3 °C/s and isothermal treatments of 400 °C show hardness values corresponding to the hardness in the wheel's tread (between 0 - 3mm in depth), where the microstructure presents a mixture of microconstituents.
- Both the microstructure and the wheel hardness at a depth of 12 mm have unique characteristics and are comparable to the microstructure and hardness of the isothermal treatment at 500 °C. This temperature is used during tempering the wheel after the quenching treatment.

#### **Acknowledgments**

The authors would like to acknowledge The Brazilian Nanotechnology National Laboratory (LNNano) for the use of equipment's (Gleeble 3800, XRD and hardness mapping). MWL Brazil for providing economic funding, and CNPq (National Council for Scientific and Technological Development) for scholarships received.

#### **References**

- [1] Y. Okagata. Desing technologies for railway wheels and future prospects. Nippon steel & Sumitomo metal technical report. p. 26-33, n. 105. 2013.

- [2] K. Wang; R. Pilon. Investigation of heat treating of railroad wheels and its effect on braking using finite element analysis. Griffin Wheel Company.
- [3] N. Zhang, J. W. Zhang, L. T. Lu, M. T. Zhang, D. F. Zeng, Q. P. Song, Q.P.: Wear and friction behavior of austempered ductile iron as railway wheel material. *Mater. Des.* **89**, 815–822 (2016). <https://doi.org/10.1016/j.matdes.2015.10.037>
- [4] Q. Li, A. Zhao. Effect of Upper Bainite on wear behaviour of high-speed wheel steel. *Tribology Letters*, V. 67, n.121. p. 1-9, 2019. <https://doi.org/10.1007/s11249-019-1239-7>.
- [5] D. J. Minicucci, S. T. Fonseca, R. L. V. Boas, et. al. Development of niobium microalloyed steel for railway wheel with pearlitic bainitic microstructure. *Materials Research*, V. 22, n. 6, p. 1-8. 2019. DOI: <http://dx.doi.org/10.1590/1980-5373-MR-2019-0324>.
- [6] L. B. Godefroid; L. P. Moreira; et. Al. Effect of chemical composition and microstructure on the fatigue crack growth resistance of pearlitic steels for railroad application. *International Journal of Fatigue*. V. 120, p. 241-253. 2019. <https://doi.org/10.1016/j.ijfatigue.2018.10.016>
- [7] A. Kumar, S. K. Makineni, A. Dutta, C. Goulas, M. Steenbergen, R. H. Petrov, J. Sietsma. Design of high-strength and damage-resistant carbide-free fine bainitic steels for railway crossing applications. *Materials Science & Engineering A*, v. 759, p. 210-223, 2019. <https://doi.org/10.1016/j.msea.2019.05.043>.
- [8] K. Cvetkovski, J. Ahlström, B. Karlsson, B.: Thermal softening of fine pearlitic steel and its effect on the fatigue behavior. *Proced. Eng.* 2, 541–545, 2010. <https://doi.org/10.1016/j.proeng.2010.03.058>.
- [9] D. Zeng, L. Lu, Y. G, et. al. Optimization of strength and toughness of railway wheel steel by alloy design. *Materials and Design*, V. 92, p.998-1006, 2016. <http://dx.doi.org/10.1016/j.matdes.2015.12.096>.
- [10] J.P. Liu, Y.Q. Li, Q.Y. Zhou, Y.H. Zhang, Y. Hu, L.B. Shi, W.J. Wang, F.S. Liu, S. B. Zhou, C.H. Tian, New insight into the dry rolling-sliding wear mechanism of carbide-free bainitic and pearlitic steel, *Wear* p. 432–433, 2019. <https://doi.org/10.1016/j.wear.2019.202943>.
- [11] W. Solano-Alvarez, E.J. Pickering, H.K.D.H. Bhadeshia, Degradation of nanostructured bainitic steel under rolling contact fatigue, *Mater. Sci. Eng., A* 617 (2014) 156–164, <https://doi.org/10.1016/J.MSEA.2014.08.071>.
- [12] O. Hajizad, A. Kumar, Z. Li, R.H. Petrov, J. Sietsma, R. Dollevoet, Influence of microstructure on mechanical properties of bainitic steels in railway applications, *Metals (Basel)* 9 (2019) 1–19, <https://doi.org/10.3390/met9070778>.
- [13] D. Zapata, J. Jaramillo, A. Toro. Rolling contact and adhesive wear of bainitic and pearlitic steels in low load regime. *Wear*, v. 271, p. 393-399, 2011. ISSN: 00431648, DOI: 10.1016/j.wear.2010.10.009.
- [14] J. P. Liu, Y. Q. Li, J. Y. Jin, et. al. Effect of processing techniques on microstructure and mechanical properties of carbide-free bainitic rail steels. *Materials Today Communications*. 2020. <https://doi.org/10.1016/j.mtcomm.2020.101531>.
- [15] F. C. Robles Hernández, S. Cummings, S. Kalay, et. al. Properties and microstructure of high performance wheels. *Wear*, V. 271, p.374-381, 2011. doi:10.1016/j.wear.2010.10.017
- [16] C. Lonsdale; S. Dedmon; J. Pitch Recent developments in forged railroad wheels for improved performance. *Proceedings of Joint Rail Conference*, p. 39 – 43. 2005 – Pueblo - CO
- [17] F. Fazeli, B. S. Amirkhiz, C. Scott, M. Arafin, L. Collins. Kinetics and microstructural change of low-carbon bainite due to vanadium microalloying. *Mater. Sci. Eng. A* **720**, 248–256 (2018). <https://doi.org/10.1016/j.msea.2018.02.042>
- [18] C. Qiu; J. Cookson; P. Mutton. The role of microstructure and its stability in performance of wheels in heavy haul service. *Journal Mod. Transport*. V. 25, n. 4, p. 261-267. 2017. DOI 10.1007/s40534-017-0143-9.
- [19] P. Molyneux-Berry, C. Davis, A. Bevan. The influence of wheel/rail contact conditions on the microstructure and hardness of railway wheels. *The Scientific World Journal*, V. 2014, p.1-16, 2014. <http://dx.doi.org/10.1155/2014/209752>.
- [20] H. K. D. H. Bhadeshia: *Bainite in steels* - 2<sup>nd</sup> ed., p. 1-460, Institute of Materials, Cambridge- UK (2001).
- [21] S. L. Miller. Effect of microalloying on the strength of high carbon wire steels. These (Ph.D.) - Department of Metallurgical and Materials Engineering, Colorado School of Mines, Golden, 2014. 96 p.
- [22] A. Ren; Y. Ji; G. Zhou, Y. Ze-Xim H. Bin, L. Yi; Hot deformation behaviour of V-microalloyed steel. *Journal of Iron and Steel Research, International*, 2010, ser. 8, vol. 17, pp. 55–60.
- [23] P. H. Shipway; S. J. Wood and A. H. Dent. The hardness and sliding wear behaviour of a bainitic steel. *Wear*, 1997, vol. 203-204, pp. 196-205.
- [24] K. Han; D. V. Edmonds; G. D. W. Smith. Optimization of mechanical properties of high-carbon pearlitic steel with Si and V additions. *Metallurgical and Materials Transactions A*, 2001, ser. 6, vol. 32, pp. 1313–1324.
- [25] R. L. Villas Boas; A. P. A. Cunha; S. T. Fonseca; M. H. Silva; P. R. Mei. Proceeding of the National Congress of Mechanical Engineer. Campina Grande, BR, 2010. vol. 1, pp. 1-10.
- [26] S. D. Bakshi; P. H. Shipway; H. K. D. H. Bhadeshia. Three-body abrasive wear of fine pearlite, nanostructured bainite and martensite. *Wear*, **308**, 46-53, 2013. <http://dx.doi.org/10.1016/j.wear.2013.09.008>.

- [27] S. T. Fonseca; A. Sinatora; A. J. Ramirez; D. J. Minicucci; C. R. Afonso; P. R. Mei: Defect and diffusion forum, **367**, 60-67, 2016. doi:10.4028/www.scientific.net/DDF.367.60.
- [28] American Association of Railroads (AAR). M107/208 Section G; 2013.
- [29] D. Rasouli; Sh. Khameneh Asl; A. Akbarzadeh; G. H. Daneshi. Effect of colling rate on the microstructure and mechanical properties of microalloyed forging steel. *Journal of Materials Processing Technology*, V. **206**, p. 92-98, 2008. doi:10.1016/j.jmatprotec.2007.12.006
- [30] J.D. Verhoeven, E. D. Gibson. The divorced eutectoid transformation in steel. *Metallurgical & Materials Transactions A*, [s.l.], v. 29, p. 1181–1189, 1998.
- [31] A. Ray. Niobium microalloying in rail steels. *Materials Science and Technology*. V. 33. N. 14. P. 1584-1600. 2017. <https://doi.org/10.1080/02670836.2017.1309111>
- [32] M. Masoumi, E. A. Echeverri, A. Tschiptschin, et. al. Improvement of wear resistance in a pearlitic rail steel via quenching and partitioning processing. *Scientific reports*, V. 9, p. 1-12. 2019. <https://doi.org/10.1038/s41598-019-43623-7>
- [33] O. P. Modi, N. Deshmukh, D. P. Mondal, A. K. Jha, A. H. Yegneswaran, K. H. Khaira. Effect of interlamellar spacing on the mechanical properties of 0.65 %C steel. *Materials Characterization*, v. 46, p. 347-352, 2001.
- [34] P.P. Senthil, K. S. Rao; H. K. Nandi, et. al. Influence of niobium microalloying on the microstructure and mechanical properties of high carbon nano bainitic steel. *Procedia Structural Integrity*, v. 14, p. 729-737, 2019. 10.1016/j.prostr.2019.05.091
- [35] T. Takahashi, W. A. Bassett, M. Hokwang. Isothermal compression of the alloys of iron up to 300 kbar at room temperature: Iron-nickel alloys. *Journal of Geophysical Research, B*, [s.l.], v. 73, p. 4717–4725, 1968.
- [36] C. Schade, T. Murphy, et. al. Microstructure and mechanical properties of a bainitic PM steels. *International Journal of Powder Metallurgy*, [s.l.], v. 48, no 3, p. 51–59, 2012. ISSN: 08887462.
- [37] C. Chattopadhyay, S. Sangal, K. Mondal, et al. Improved wear resistance of medium carbon microalloyed bainitic steels. *Wear*, [s.l.], v. 289, p. 168–179, 2012. ISSN: 0043-1648, DOI: 10.1016/J.WEAR.2012.03.005.
- [38] H. N. El-Din. et al. Structure-properties relationship in trip type bainitic ferrite steel austempered at different temperatures. *International Journal of Mechanical and Materials Engineering*, [s.l.], v. 12, no 1, p. 1–9, 2017. ISSN: 18230334, DOI: 10.1186/s40712-017-0071-9.
- [39] K. F. Rodrigues, G. M. M. Mourão, G. L. Faria. Kinetics of isothermal phase transformations in premium and stardard rail steels. *Steel Research*, v. 8, 2020. <https://doi.org/10.1002/srin.202000306>
- [40] S. Sharma, S. Sangal, K. Mondal. Wear behavior of bainitic rail and wheel steel. *Materials Science and Technology*, V. 32:4, p. 266-274, 2016. <http://dx.doi.org/10.1080/02670836.2015.1112537>
- [41] J. Yin, M. Hillert, A. Borgenstam. Morphology of Upper and Lower Bainite with 0.7 Mass pct C. *Metallurgical and Materials Transactions A*. v. 48A. p. 4006-4024. 2017. DOI: 10.1007/s11661-017-4208-5
- [42] F. G. Caballero, M. J. Santofimia, C Garcia-Mateo, C. G Andrés. Time-temperature-transformation Diagram within the bainitic temperature range in a medium carbon steel. *Materials Transactions*, v. 45, n. 12, p. 3272-3281, 2004.
- [43] S. Zajac, V. Schwinn, H. Tacke. Characterization and quantification of complex bainitic microstructures in high and ultra-high strength linepipe steels. *Materials Science Forum*. V.500-501, p. 388-394, 2005. DOI: [10.4028/www.scientific.net/MSF.500-501.387](https://doi.org/10.4028/www.scientific.net/MSF.500-501.387)
- [44] J. Debehets, J. Tacq, A. Favache, et. al. Analysis of the variation in nanohardness of pearlitic steel: Influence of the interplay between ferrite crystal orientation and cementite morphology. *Materials Science & Engineering A*, V. 616, p. 99-106, 2014. <http://dx.doi.org/10.1016/j.msea.2014.08.019>.
- [45] H. Lan, L. Du, N. Zhou, et. al. Effect of austempering route on microstructural characterization of nanobainitic steel. *Acta Metallurgica Sinica*. V. 27, n. 1, p. 19-26, 2014. DOI 10.1007/s40195-013-0006-2.
- [46] C. Liu, R. Ren, D. Zhao, C. Chen, An EBSD investigation on the evolution of the surface microstructure of D2 wheel steel during rolling contact fatigue, *Tribology Letter*. 68 (2020) 11, <https://doi.org/10.1007/s11249-020-1277-1>
- [47] Y. Hu, L. Zhou, H.H. Ding, R. Lewis, Q.Y. Liu, J. Guo, W.J. Wang. Microstructure evolution of railway pearlitic wheel steels under rolling-sliding contact loading, *Tribology International*, 106685, 2020, <https://doi.org/10.1016/j.triboint.2020.106685>.
- [48] J. Kalousek, D. M. Fegredo, E. E. Laufer. The wear resistance and worn metallografy of pearlite, bainite and tempered martensite rail steel microstructures of high hardness. *Journal on the Science and Technology of friction lubrication and wear*, v. 105, p. 199-222, 1985. DOI: 10.1016/0043-1648(85)90068-7.